

NASA

MEMORANDUM

EXPLORATORY INVESTIGATION OF THE LONGITUDINAL AERODYNAMIC
CHARACTERISTICS OF A CANARD AIRPLANE CONFIGURATION
AT A MACH NUMBER OF 2.98

By Robert W. Dunning

Langley Research Center
Langley Field, Va.

FACILITY FORM 602

N 71-72103
(ACCESSION NUMBER)
24
(PAGES)
(NASA CR OR TMX OR AD NUMBER)
(THRU)
None
(CODE)
(CATEGORY)

CLASSIFICATION CHANGED
[REDACTED]TO: NASA
Authority of TD 7122 Date 3-30-71

NATIONAL AERONAUTICS AND SPACE ADMINISTRATION

WASHINGTON

October 1958

K

[REDACTED]

NATIONAL AERONAUTICS AND SPACE ADMINISTRATION

NASA MEMO 10-6-58L

EXPLORATORY INVESTIGATION OF THE LONGITUDINAL AERODYNAMIC
CHARACTERISTICS OF A CANARD AIRPLANE CONFIGURATION

AT A MACH NUMBER OF 2.98*

By Robert W. Dunning

SUMMARY

An exploratory investigation has been conducted at a Mach number of 2.98 to determine the maximum lift-drag ratio attainable with a canard airplane configuration incorporating favorable lift interference with a shaped fuselage to increase configuration lift. The tests were conducted at an average Reynolds number of 3.5×10^6 based on wing mean aerodynamic chord through an angle-of-attack range from -10° to 10° . The results indicate that a maximum lift-drag ratio of 6.3 has been obtained with this type of configuration and further increases may be realized with further model refinements.

INTRODUCTION

In the design of an efficient long-range supersonic-airplane configuration, it is necessary to provide a sufficient volume to enclose such items as the crew, fuel, powerplant, and payload, and at the same time generate a reasonably high lift-drag ratio, L/D . References 1 to 5 suggest the use of favorable interference effects to increase L/D ; however, the configurations resulting from designing by interference considerations are usually quite different from current airplane shapes and, as yet, have not been fully investigated. In references 6 to 8 the fuselage is shaped to make it a better generator of lift. The present exploratory tests were undertaken to see whether perhaps some of the features of both approaches might be combined to give a practical configuration having a high L/D . Breakdown tests were conducted at a Mach number of 2.98 at an average Reynolds number of 3.5×10^6 based on wing mean aerodynamic chord. Lift, drag, and pitching moment were obtained at $\beta = 0$ through an angle-of-attack range from -10° to 10° .

[REDACTED]


[REDACTED]

Inasmuch as the tests were of an exploratory nature, no data were obtained on control characteristics or internal-flow characteristics. Control data for this configuration can be found in references 9 and 10.

SYMBOLS

The data were obtained with respect to the body axes (fig. 1) and are plotted with respect to both the body axes and the stability axes. The reference center of gravity is located at 25 percent of the wing mean aerodynamic chord.

b	wing span
C_A	axial-force coefficient (corrected so that base pressure is equal to stream static pressure), $-F_X/qS$
C_D	drag coefficient, $C_N \sin \alpha + C_A \cos \alpha$
C_L	lift coefficient, $C_N \cos \alpha - C_A \sin \alpha$
C_m	pitching-moment coefficient, $M_Y/qS\bar{c}$
$C_{m,o}$	pitching-moment coefficient at $C_L = 0$
C_N	normal-force coefficient, $-F_Z/qS$
c	chord
\bar{c}	wing mean aerodynamic chord
F_X	force along X-axis
F_Z	force along Z-axis
L/D	lift-drag ratio
$(L/D)_{\max}$	maximum lift-drag ratio
M	Mach number
M_Y	moment about Y-axis
q	dynamic pressure



R	Reynolds number
S	wing plan-form area
t	thickness
α	angle of attack (0° when undersurface of wing is aligned with stream)
β	angle of sideslip
Λ_{le}	leading-edge sweep angle

APPARATUS


The tests were conducted in the Langley high Mach number jet. The settling-chamber pressure, which was held constant by a pressure-regulating valve, and the corresponding air temperature were continuously recorded during each run. A sting-mounted external strain-gage balance (shielded from the stream) which measured normal force, pitching moment, and axial force was used to obtain the data. Base pressures were measured on a mercury manometer board.

MODELS

Three-view drawings of the models are shown in figures 2 and 3 and photographs of the model are given as figure 4. The wing has a 0° trailing-edge-sweep trapezoidal plan form with a $2\frac{1}{2}$ -percent-thick half-double-wedge section with maximum thickness occurring at the 70-percent-chord station. The lower surface of the wing is flat and parallel to the airstream at $\alpha = 0^\circ$. Ventral fins having wedge sections are attached to the wing tips and mounted with the outboard surfaces of the fins parallel to the airstream.

The canard control has a delta plan form, a double-wedge section, and 62° leading-edge sweep. The maximum thickness is $2\frac{1}{2}$ percent located at the 70-percent-chord position. For all model configurations in which the canard was used, its angle of incidence was maintained at 0° .

The forebody of the configuration varies in cross section from a 2 to 1 ellipse over the forward portion to a combination of a half-ellipse and rectangle farther rearward. The upper body line fairs into the wing upper surface at the maximum thickness station (fig. 2).



Two underbodies (fig. 3) designated as "ducted" and "wedge" were tested. The overall height and width of the ducted underbody were determined by consideration of full-scale engine dimensions. The wedge underbody had no provisions for air flow through it and had the same depth and trailing-edge span as the ducted underbody. The ducted underbody had straight through air passages which were open for all tests.

A prism was mounted in that portion of the forebody over the upper surface of the wing (fig. 4) to indicate angle of attack.

TESTS

The tests were conducted at a Mach number of 2.98. The settling-chamber stagnation temperature during any single run varied from approximately 60° F to 40° F, and the settling-chamber stagnation pressure was held constant by a pressure regulating valve at approximately 70 pounds per square inch absolute. This pressure and temperature resulted in an average Reynolds number of approximately 3.5×10^6 based on the wing mean aerodynamic chord. The tests were conducted with air having less than 5×10^{-6} pounds of water vapor per pound of dry air which was dry enough to eliminate the effects of water condensation. The angle-of-attack range was limited by the balance maximum loads and varied from approximately -10° to 10° for zero angle of sideslip.

PRECISION OF DATA

The maximum probable uncertainties involved in the measurement of the angles and force and moment coefficients are as follows:

α	±0.2
C_N	±0.003
C_A	±0.001
C_m	±0.004

PRESENTATION OF DATA

Configuration	Information	Figure
$\Lambda_{le} = 65^\circ$; ducted underbody	Boundary-layer transition visualization	5
$\Lambda_{le} = 62^\circ$; ducted underbody	Force tests; configuration breakdown	6
$\Lambda_{le} = 65^\circ$; ducted underbody	Force tests; configuration breakdown	7
$\Lambda_{le} = 62^\circ$; wedge underbody	Force tests; configuration breakdown	8
$\Lambda_{le} = 65^\circ$; wedge underbody	Force tests; configuration breakdown	9
Complete configurations	Effects of sweep and underbody configuration	10
Configurations with canard off	Effects of sweep and underbody configuration	11
Configurations with canard off and forebody off	Effects of sweep and underbody configuration	12
Configurations with canard off, forebody off, and wing off	Effects of underbody configuration	13

RESULTS AND DISCUSSION

All tests were made with natural transition since boundary-layer visualization results (fig. 5) indicated early transition on all surfaces except the canards on which the boundary layer appeared to be laminar. Tests made with the prism cavity both unfilled (see section entitled "Models") and filled showed no appreciable effect on any of the components (figs. 6 and 9). Therefore, most of the tests were conducted with the prism cavity unfilled.

Lift

Effect of wing sweep.- There is little or no effect on lift coefficient due to changing the wing leading-edge sweep from 62° to 65° (figs. 6 to 9).

Effect of underbody.- The wedge underbody yielded slightly higher lifts than the ducted underbody (figs. 6 to 9) probably because with the wedge underbody more of the wing lower surface is exposed to the interference flow field. The increase in lift as a result of the interference effects of the underbody and tip ventrals can be determined by comparing the results of the configurations with the canard off and forebody off (figs. 6 to 9) with linear theory. (Ref. 11 shows that linear theory gives good predictions of wing lift-curve slope at this Mach number.) For example, the experimental lift-curve slope for the wing with 62° leading-edge sweep and ducted underbody is about 0.029 (fig. 6) compared with a linear-theory value for the wing alone without ventral fin tips of 0.021.

Effect of forebody and canards.- The increment in lift due to the addition of forebody and canard varied with angle of attack and configuration shape. The maximum increment was obtained on the configuration having the wing with 62° leading-edge sweep and ducted underbody. For this configuration, the canard plus forebody (including all interference effects) contribution to the total lift varied from 19 percent at $\alpha = 2^\circ$ to 16 percent at $\alpha = 9^\circ$.

Drag

Variations in wing sweep or underbody shape had little effect on the drag coefficient (figs. 6 to 9). The approximate contributions of the various components to minimum drag of the complete configuration were as follows: underbody, 45 percent; wing plus wing underbody interference, 39 percent; forebody (assuming no interference effects), 8 percent; canard plus forebody canard interference effects, 8 percent. It is interesting to note that longitudinal control and a significant portion of the total volume (forebody) can be obtained with only a small contribution to minimum drag (approximately 16 percent).

Pitching moment

The pitching-moment variation of the complete configurations indicates approximately neutral stability and a slight nonlinearity throughout the angle-of-attack range of the tests (fig. 10). This nonlinearity seems to come mainly from the wing-underbody combination (figs. 10 to 13).

As a by-product of the wing-underbody interference, a zero-lift pitching moment $C_{m,o}$ (fig. 10) is obtained for both the ducted and wedge underbodies that varies from -0.001 to -0.010, the value depending on the configuration.

Maximum Lift-Drag Ratio

There was little effect on maximum lift-drag ratio of varying the wing sweep, underbody configuration, or adding the forebody and canard. This is to be expected since these parameters had little effect on the separate components of L/D . The maximum lift-drag ratio for the complete ducted configuration was about 6.3. Since these tests were only preliminary in nature, this value of 6.3 includes the internal duct drag which is normally charged to the engines. On the other hand, no boundary-layer diverter or bleed is incorporated in the model with its attendant drag. Data presented in references 9 and 10, where a boundary-layer diverter is incorporated and duct drag is measured, indicate the same value of $(L/D)_{max}$ as obtained in the present tests, this agreement denoting that the results of the two effects may be compensating. Other factors - such as, the size of the lateral controls and the negative value of $C_{m,o}$ - should be investigated to determine whether larger values of $(L/D)_{max}$ can be obtained.




CONCLUDING REMARKS

At a Mach number of 3 and a Reynolds number of 3.5×10^6 based on wing mean aerodynamic chord, a maximum lift-drag ratio of 6.3 has been obtained with a canard airplane configuration. Further increases may be realized with further refinements.

Langley Research Center,
National Aeronautics and Space Administration,
Langley Field, Va., July 25, 1958.

REFERENCES

1. Rossow, Vernon J.: A Theoretical Study of the Lifting Efficiency at Supersonic Speeds of Wings Utilizing Indirect Lift Induced by Vertical Surfaces. NACA RM A55L08, 1956.
2. Migotsky, Eugene, and Adams, Gaynor J.: Some Properties of Wing and Half-Body Arrangements at Supersonic Speeds. NACA RM A57E15, 1957.
3. Syvertson, Clarence A., Wong, Thomas J., and Gloria, Hermilo R.: Additional Experiments With Flat-Top Wing-Body Combinations at High Supersonic Speeds. NACA RM A56I11, 1957.
4. Ferri, Antonio, Clarke, Joseph H., and Casaccio, Anthony: Drag Reduction in Lifting Systems by Advantageous Use of Interference. PIBAL Rep. No. 272 (Contract AF 18(600)-694), Polytechnic Inst. Brooklyn, May 1955.
5. Reyn, John W., and Clarke, Joseph H.: An Assessment of Body Lift Contributions and of Linearized Theory for Some Particular Wing-Body Configurations. PIBAL Rep. No. 305 (Contract No. AF 18(600)-693), Polytechnic Inst. Brooklyn, June 1956. (Available from ASTIA as Document No. AD-96511.)
6. Hasel, Lowell E., and Kouyoumjian, Walter L.: Investigation of Static Pressures and Boundary-Layer Characteristics on the Forward Parts of Nine Fuselages of Various Cross-Sectional Shapes at $M_\infty = 2.01$. NACA RM L56I13, 1957.
7. Carlson, Harry W., and Gapcynski, John P.: An Experimental Investigation at a Mach Number of 2.01 of the Effects of Body Cross-Section Shape on the Aerodynamic Characteristics of Bodies and Wing-Body Combinations. NACA RM L55E23, 1955.
8. Jorgensen, Leland H.: Elliptic Cones Alone and With Wings at Supersonic Speeds. NACA TN 4045, 1957.
9. Kelly, Thomas C., Carmel, Melvin M., and Gregory, Donald T.: An Exploratory Investigation at Mach Numbers of 2.50 and 2.87 of a Canard Bomber-Type Configuration Designed for Supersonic Cruise Flight. NACA RM L58B28, 1958.
10. Baals, Donald D., Toll, Thomas A., and Morris, Owen G.: Airplane Configurations for Cruise at a Mach Number of 3. NACA RM L58E14a, 1958.

- 
11. Kaattari, George E.: Pressure Distributions on Triangular and Rectangular Wings to High Angles of Attack - Mach Numbers 2.46 and 3.36. NACA RM A54J12, 1955.
- 
- 

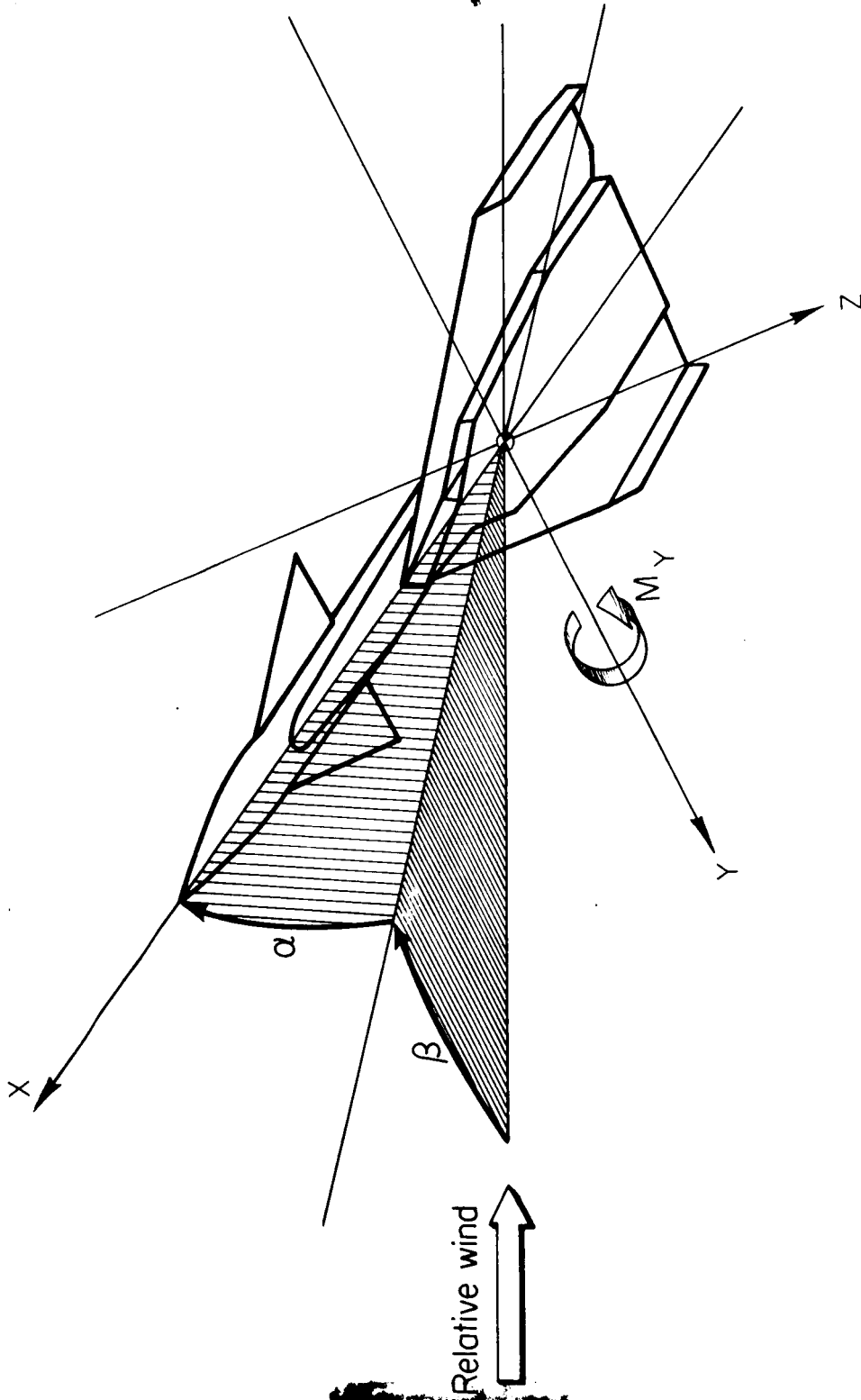
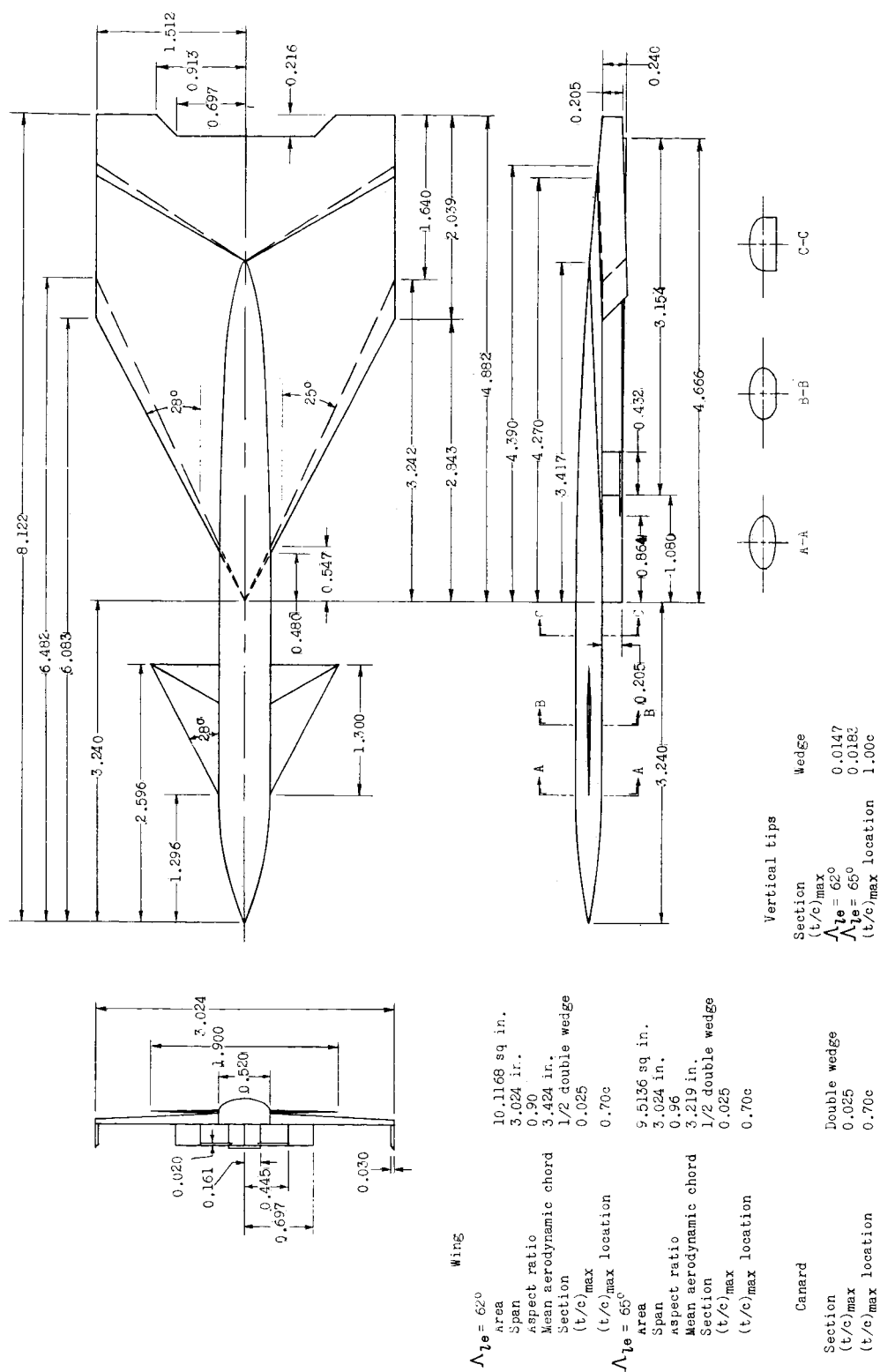


Figure 1.- System of body axes.



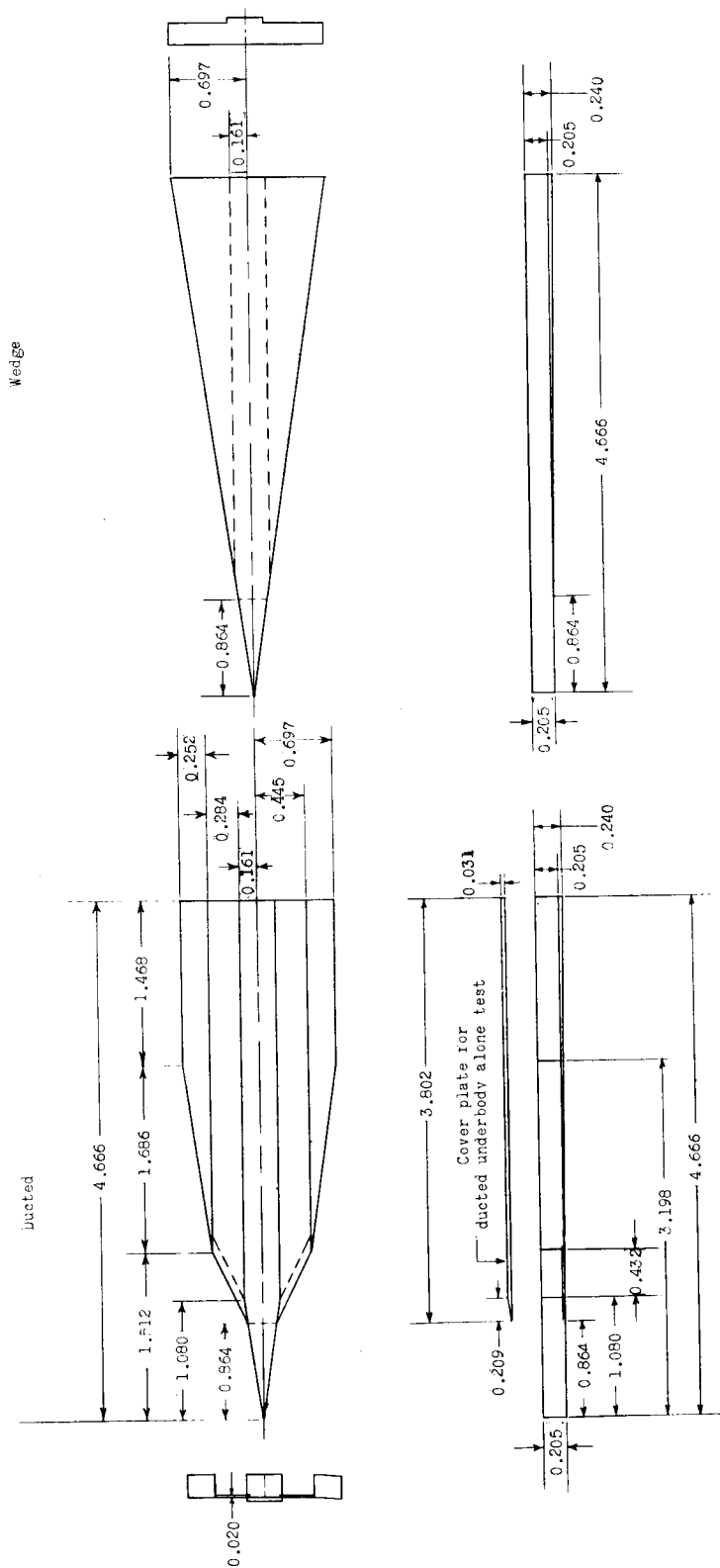
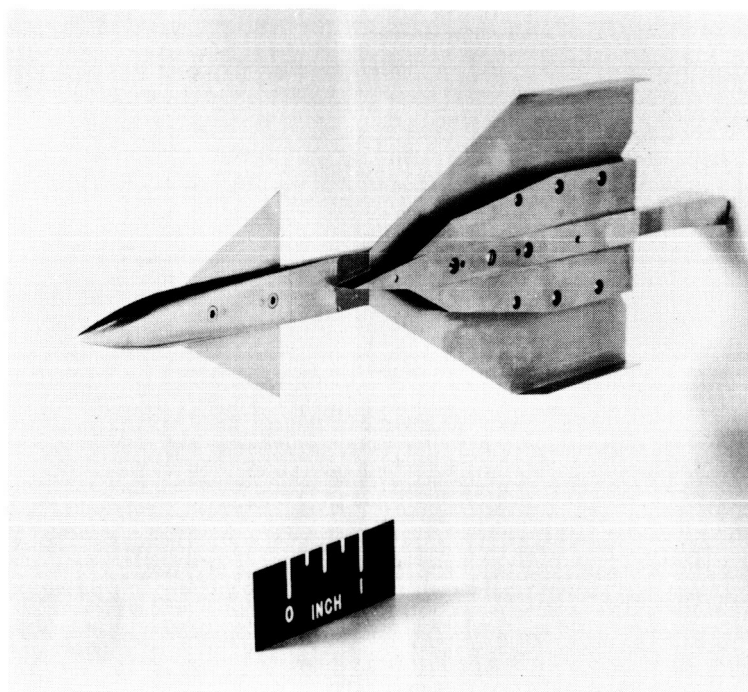
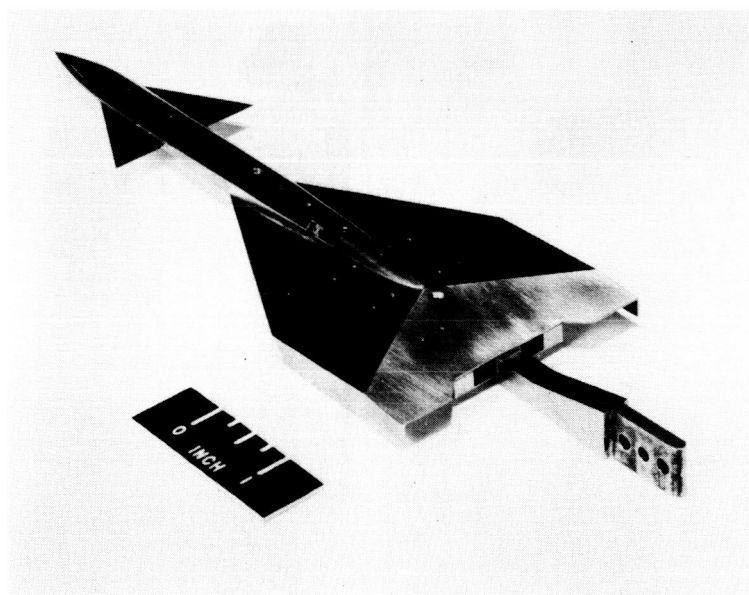


Figure 3.- Details of underbodies. (All dimensions are in inches.)

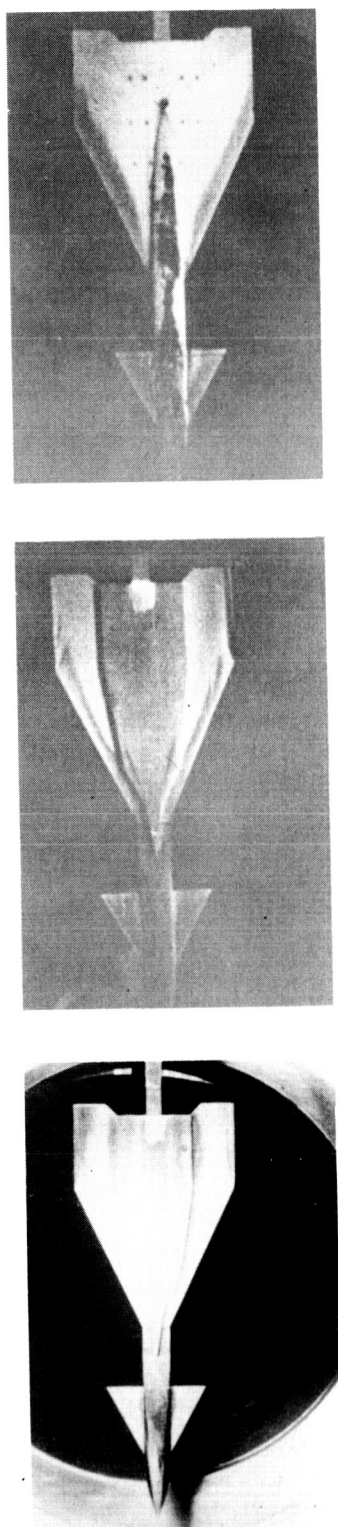


L-57-3518



L-57-3515

Figure 4.- Model tested in Langley high Mach number jet. Wing leading-edge sweep, 62° ; ducted underbody.



Forebody and Canard

Wing lower surface

Wing upper surface

L-58-2521
 Figure 5.- Location of boundary-layer transition on canard bomber model in Langley high Mach number jet. $M = 2.98$; $R = 3.5 \times 10^6$ based on wing mean aerodynamic chord; $\Lambda_{le} = 65^\circ$; $\alpha = 0^\circ$; $\beta = 0^\circ$.

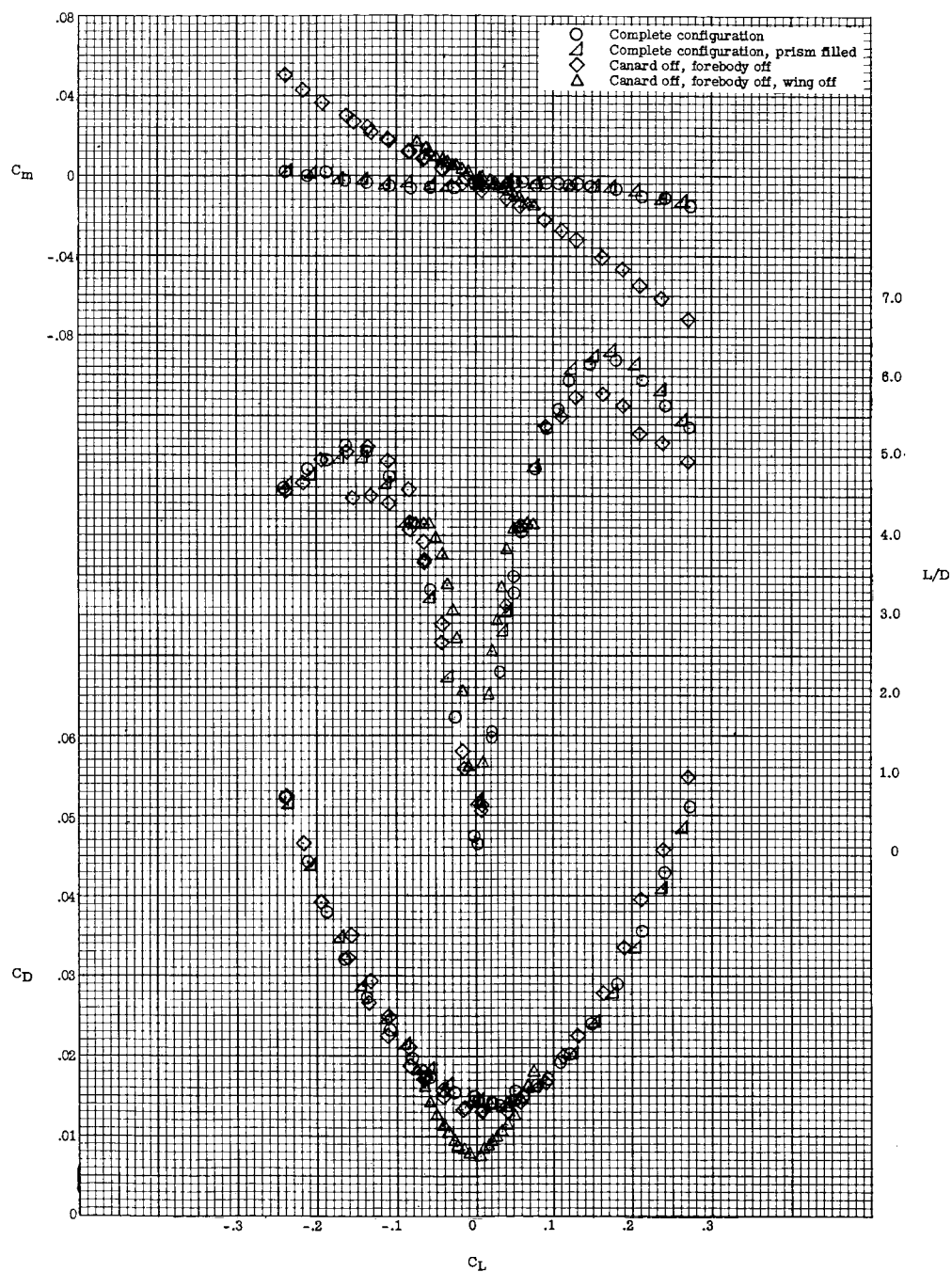


Figure 6.- Longitudinal aerodynamic characteristics of the configuration with ducted underbody and wing having 62° leading-edge sweep. $\beta = 0^\circ$; $M = 2.98$; $R = 3.5 \times 10^6$ based on wing mean aerodynamic chord.

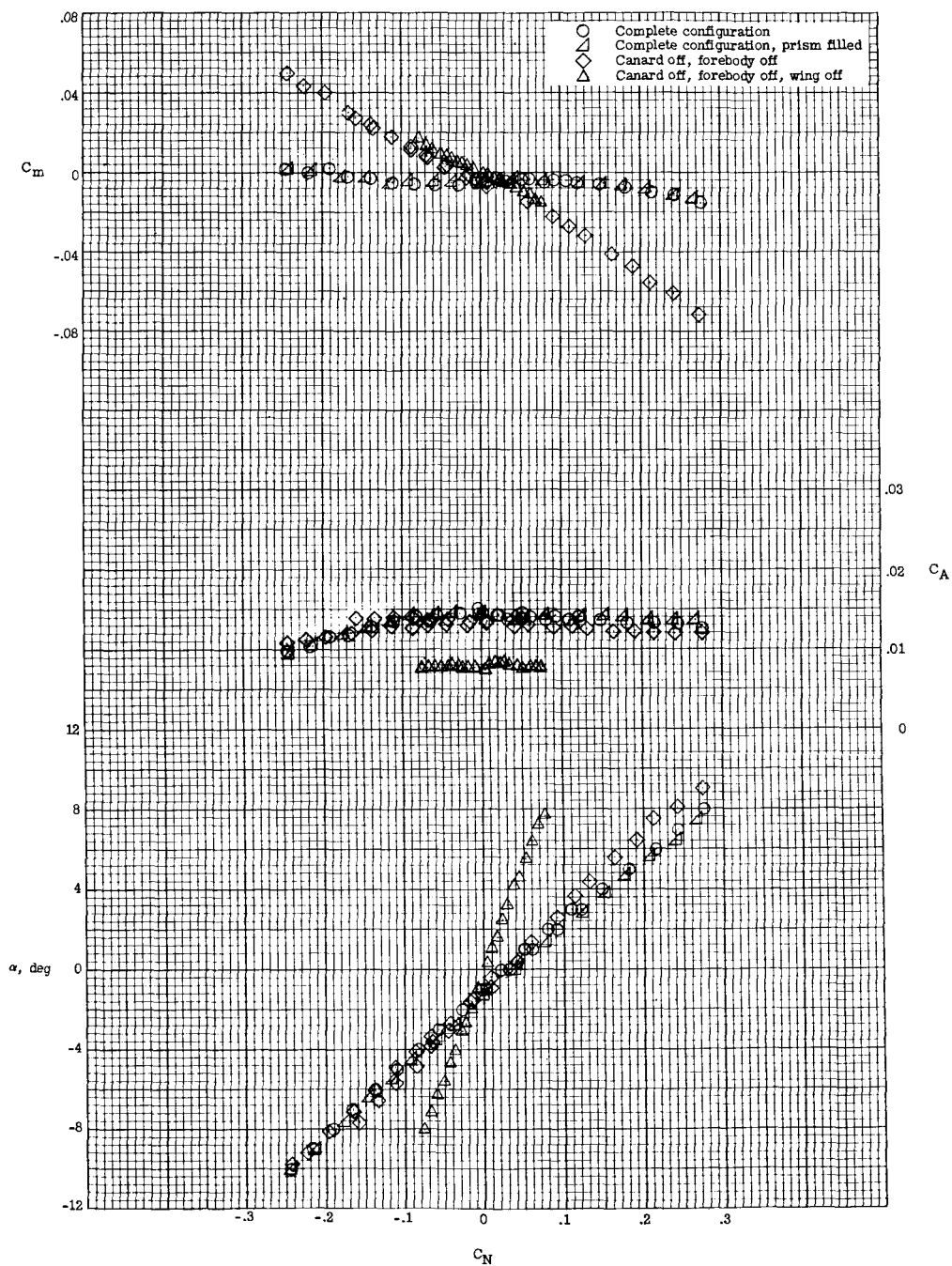


Figure 6.- Concluded.

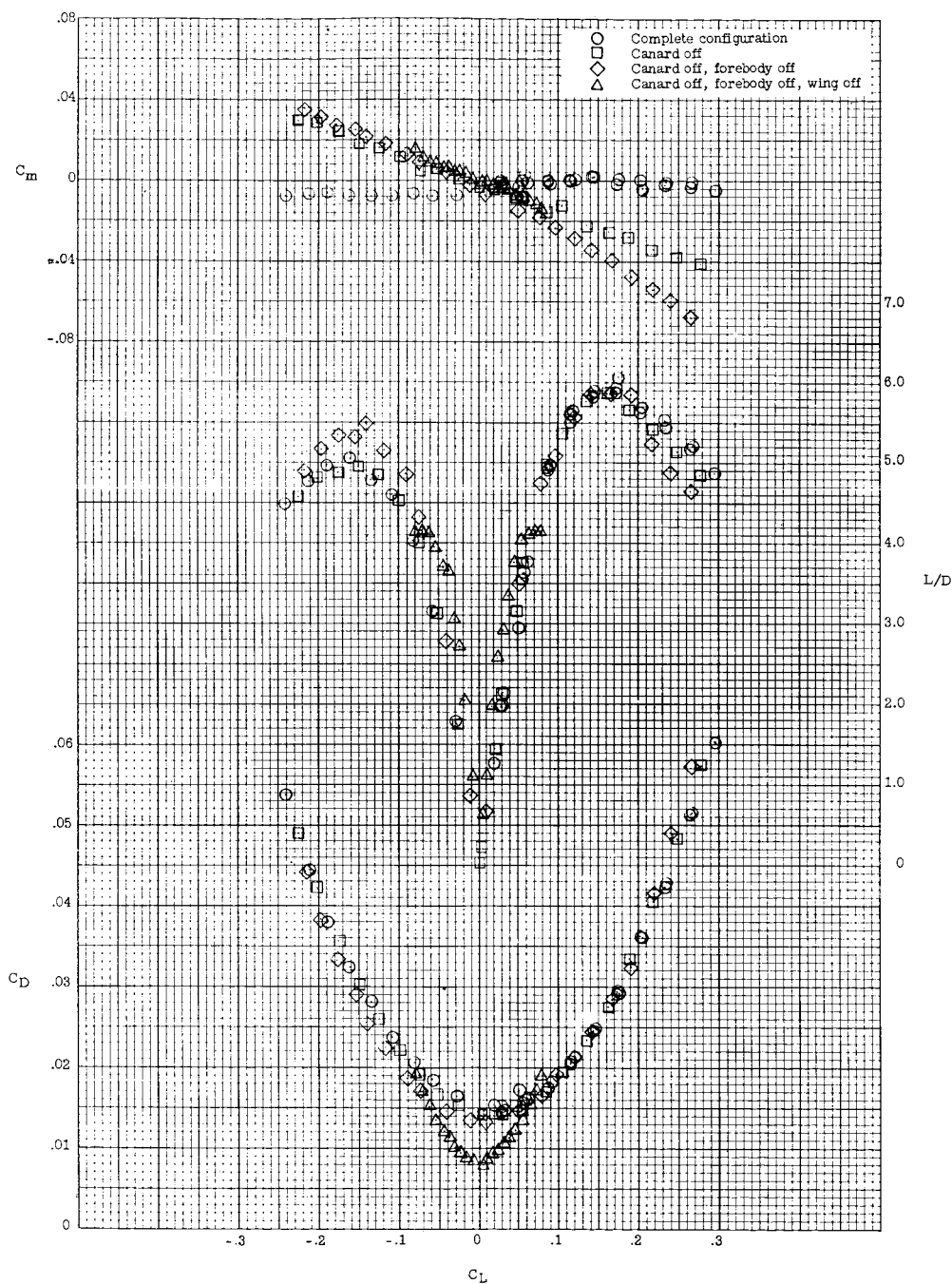


Figure 7.- Longitudinal aerodynamic characteristics of the configuration with ducted underbody and wing having 65° leading-edge sweep. $\beta = 0^\circ$; $M = 2.98$; $R = 3.5 \times 10^6$ based on wing mean aerodynamic chord.

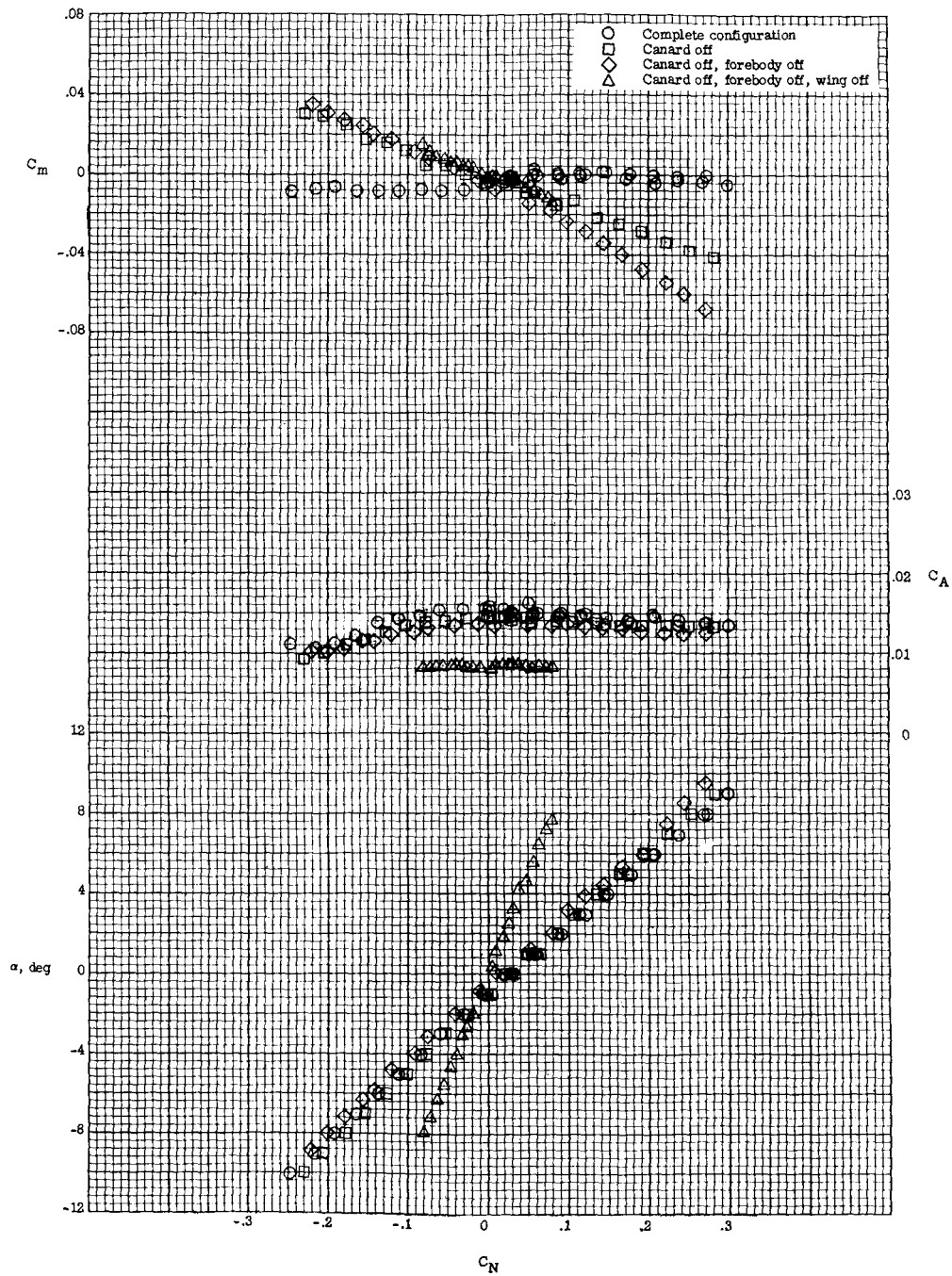


Figure 7.- Concluded.

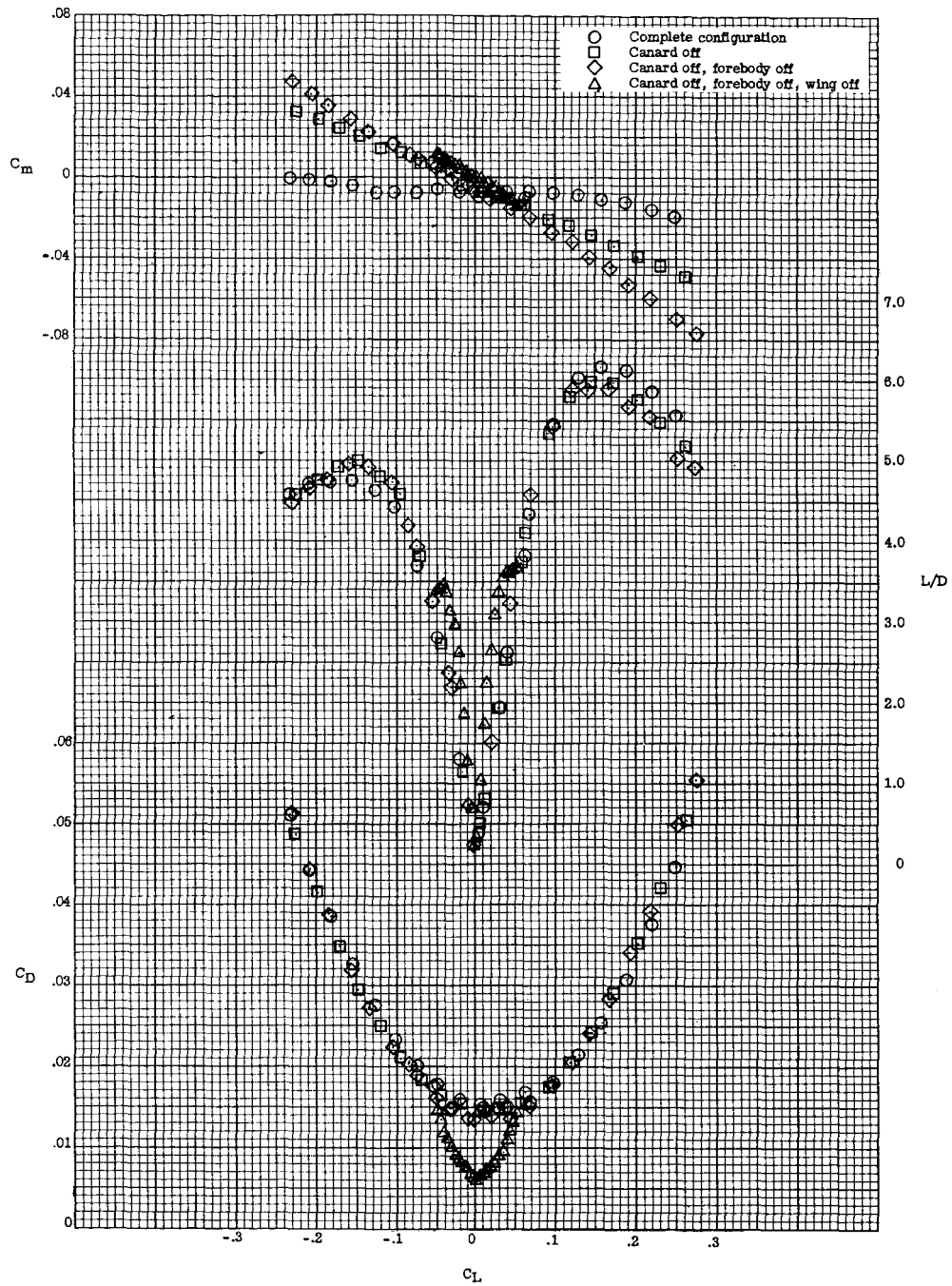


Figure 8.- Longitudinal aerodynamic characteristics of the configuration with wedge underbody and wing having 62° leading-edge sweep.

$\beta = 0^\circ$; $M = 2.98$; $R = 3.5 \times 10^6$ based on wing mean aerodynamic chord.

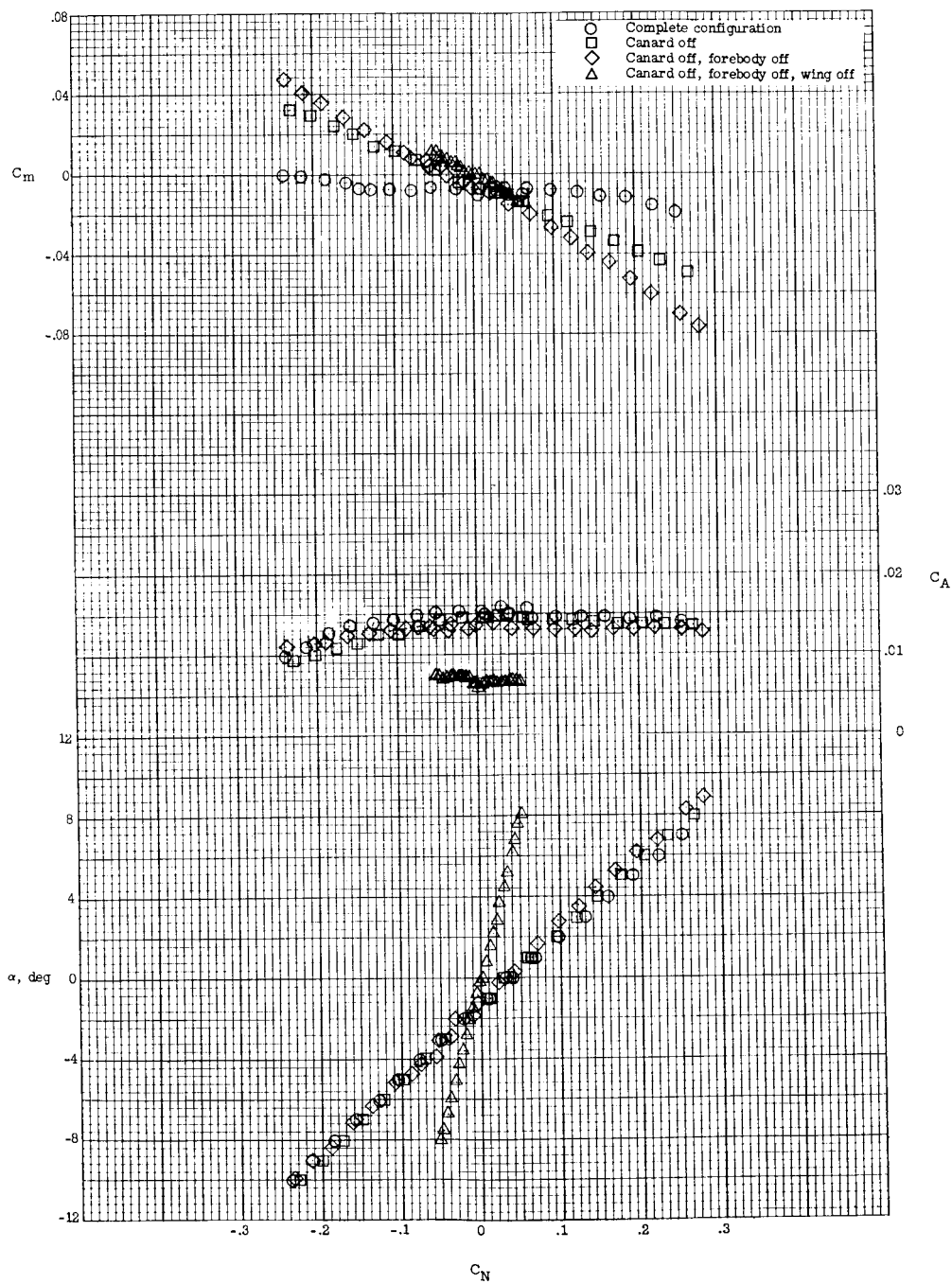


Figure 8.- Concluded.

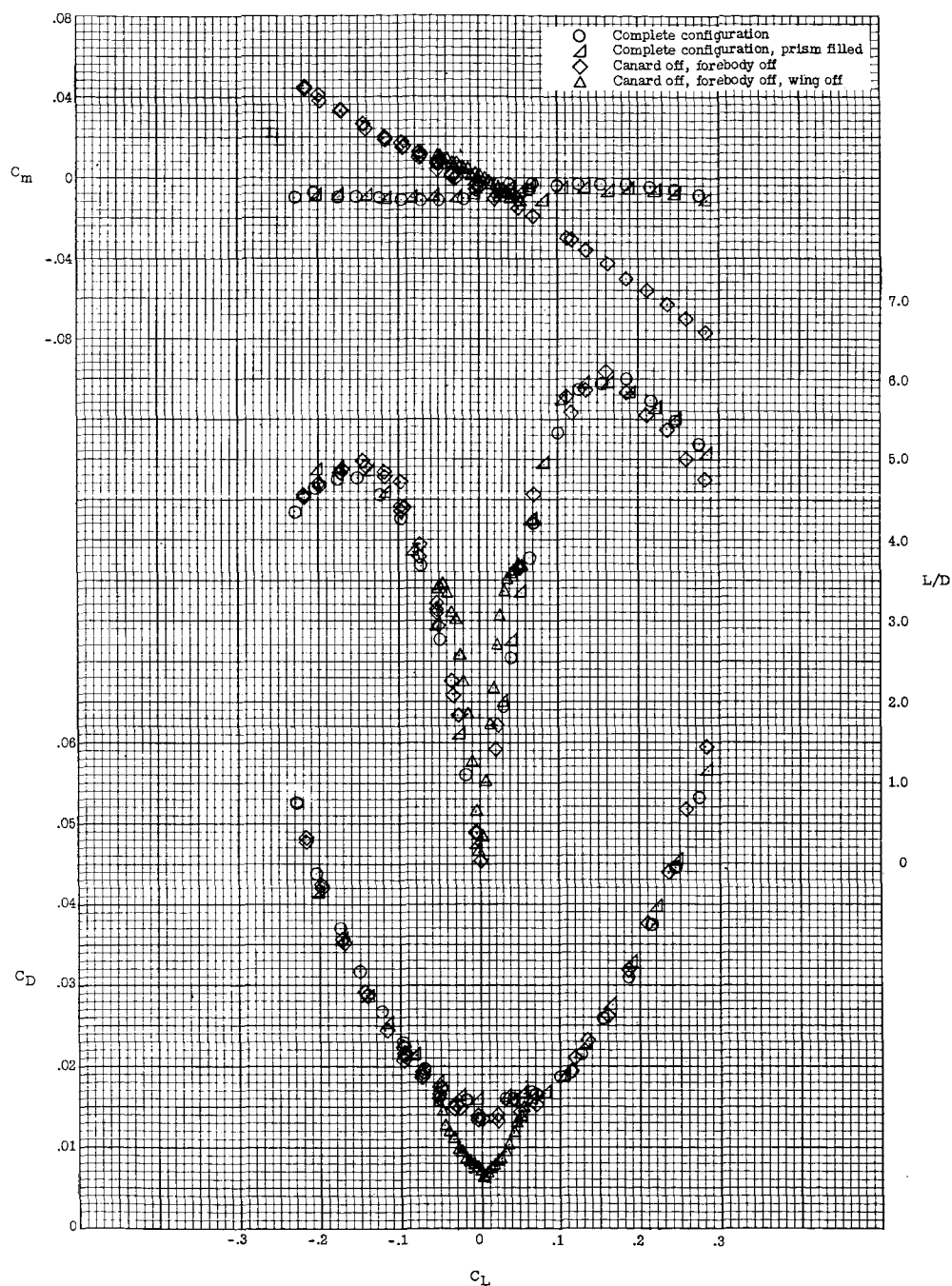


Figure 9.- Longitudinal aerodynamic characteristics of the configuration with wedge underbody and wing having 65° leading-edge sweep. $\beta = 0^\circ$; $M = 2.98$; $R = 3.5 \times 10^6$ based on wing mean aerodynamic chord.

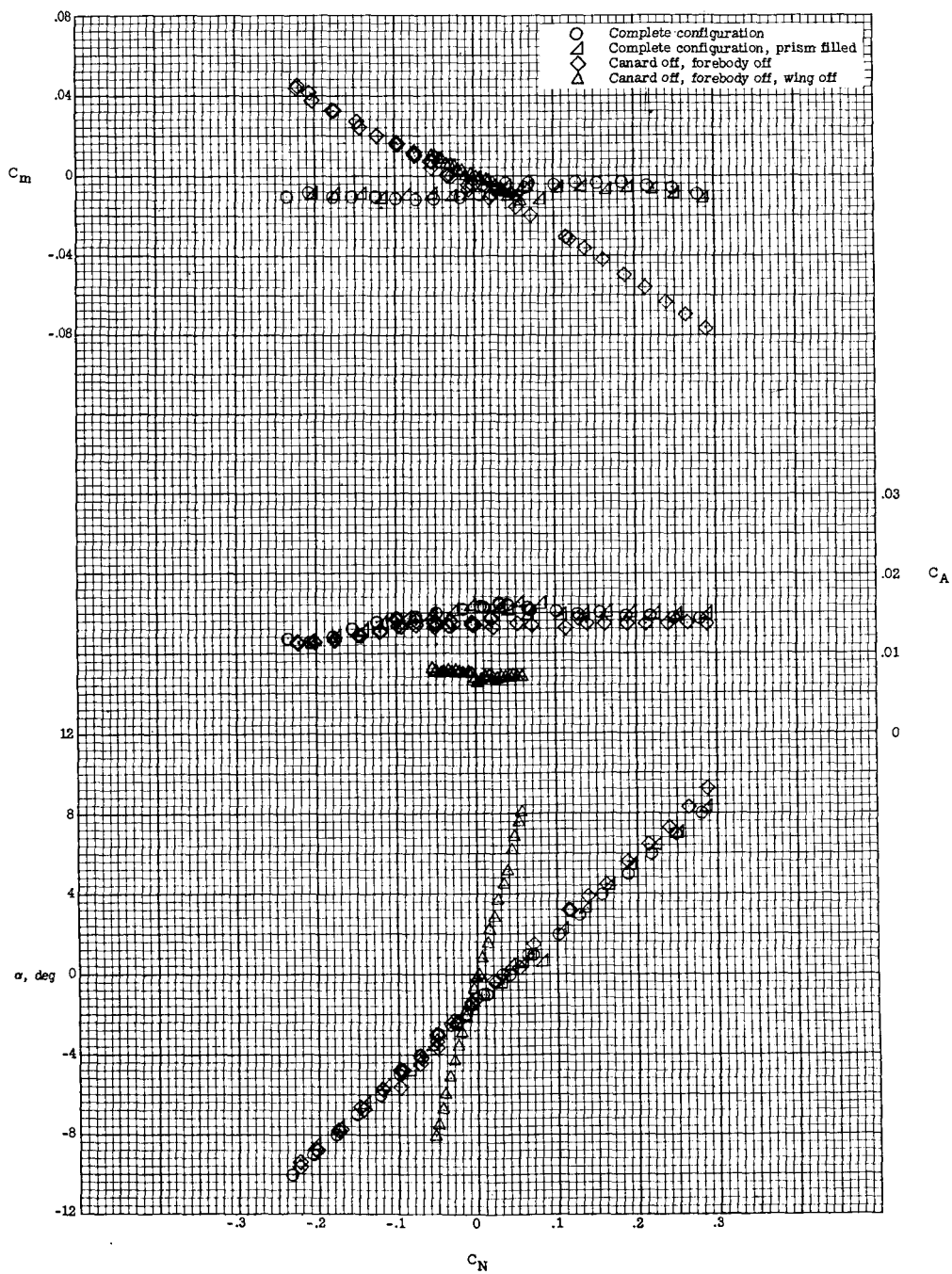


Figure 9.- Concluded.

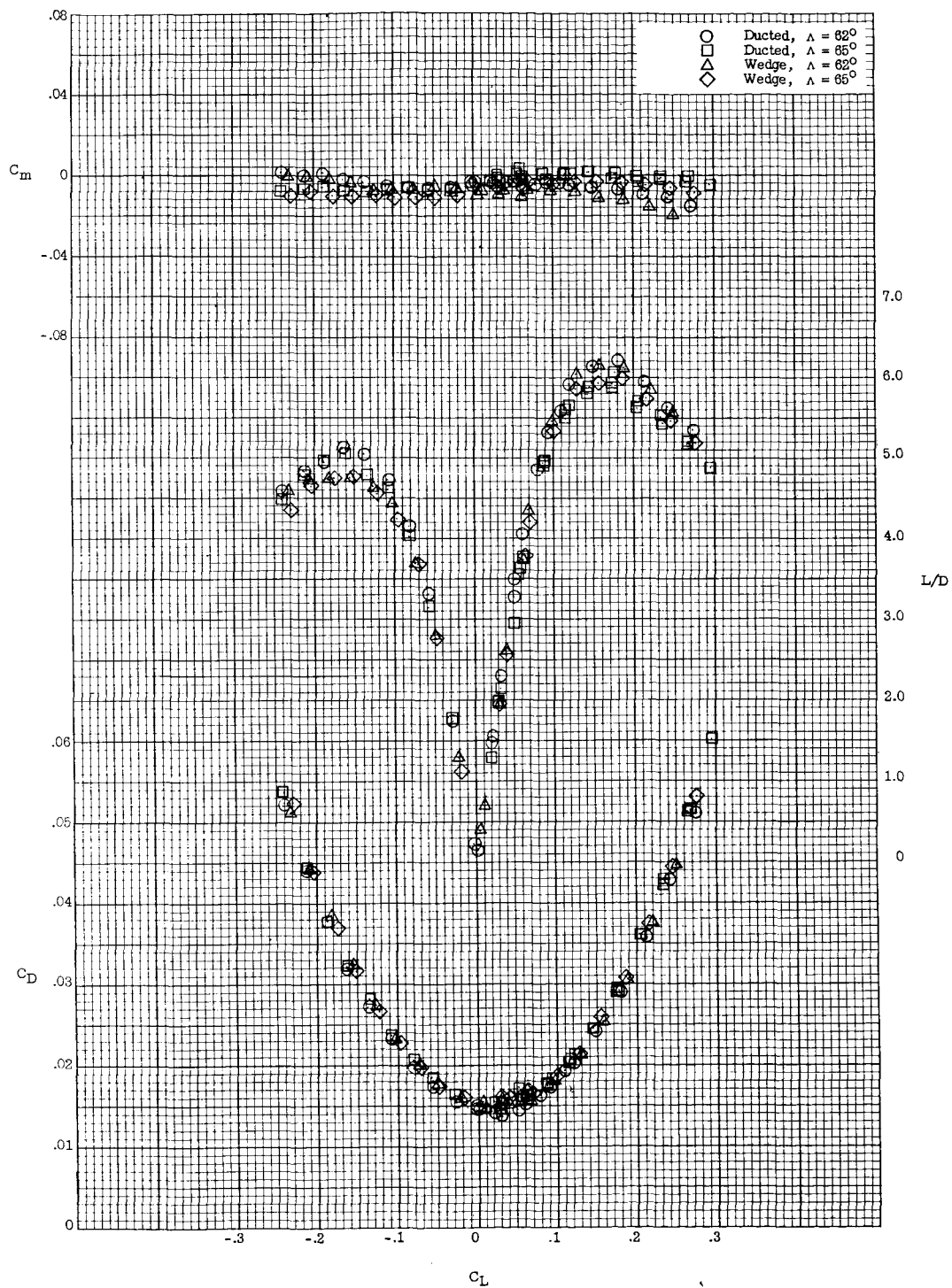


Figure 10.- Comparison of the complete configurations. $\beta = 0^\circ$; $M = 2.98$;
 $R = 3.5 \times 10^6$ based on wing mean aerodynamic chord.

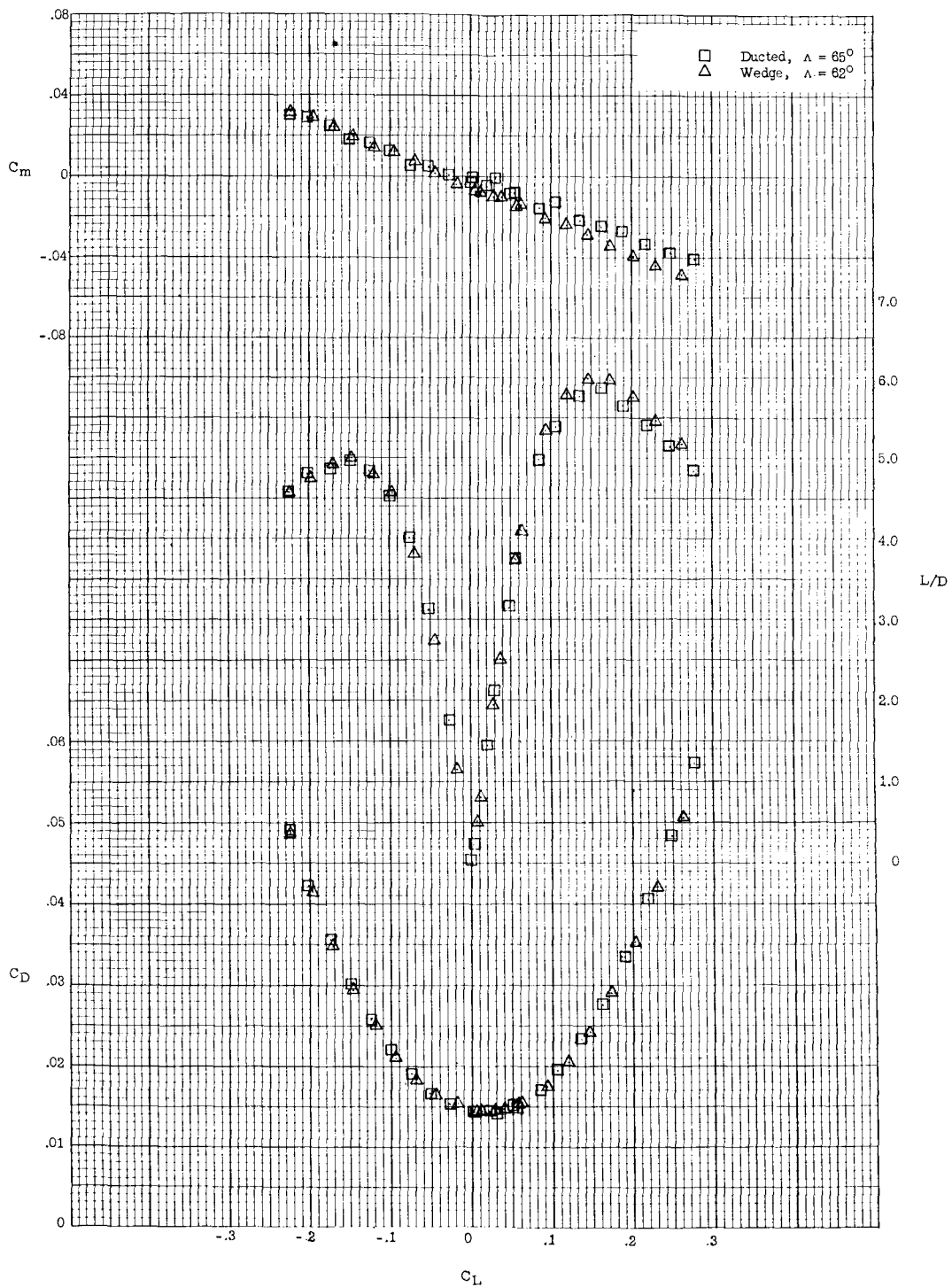


Figure 11.- Comparison of the configurations with canard off. $\beta = 0^\circ$; $M = 2.98$; $R = 3.5 \times 10^6$ based on wing mean aerodynamic chord.

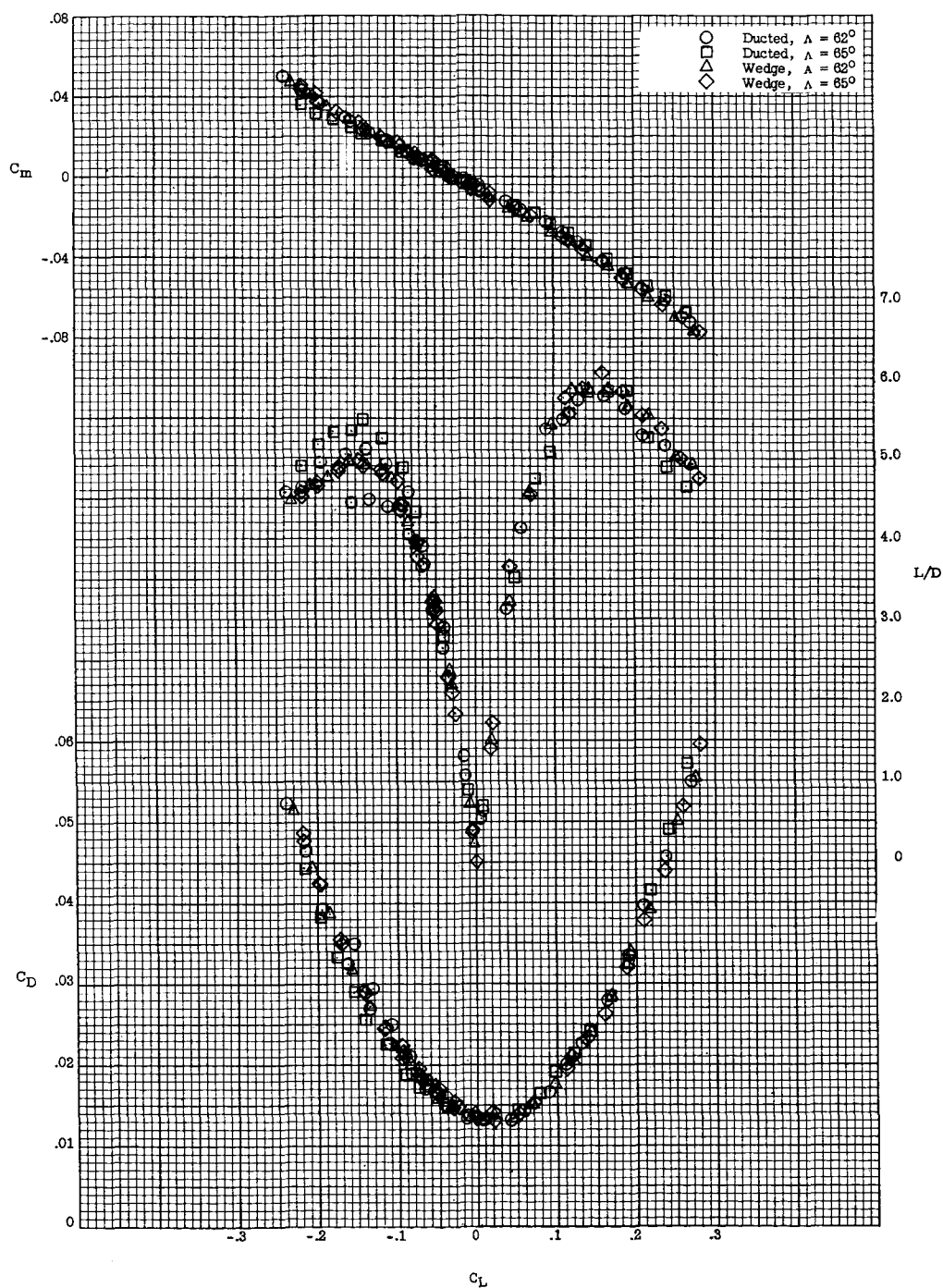


Figure 12.- Comparison of the configurations with canard off and forebody off. $\beta = 0^\circ$; $M = 2.98$; $R = 3.5 \times 10^6$ based on wing mean aerodynamic chord.

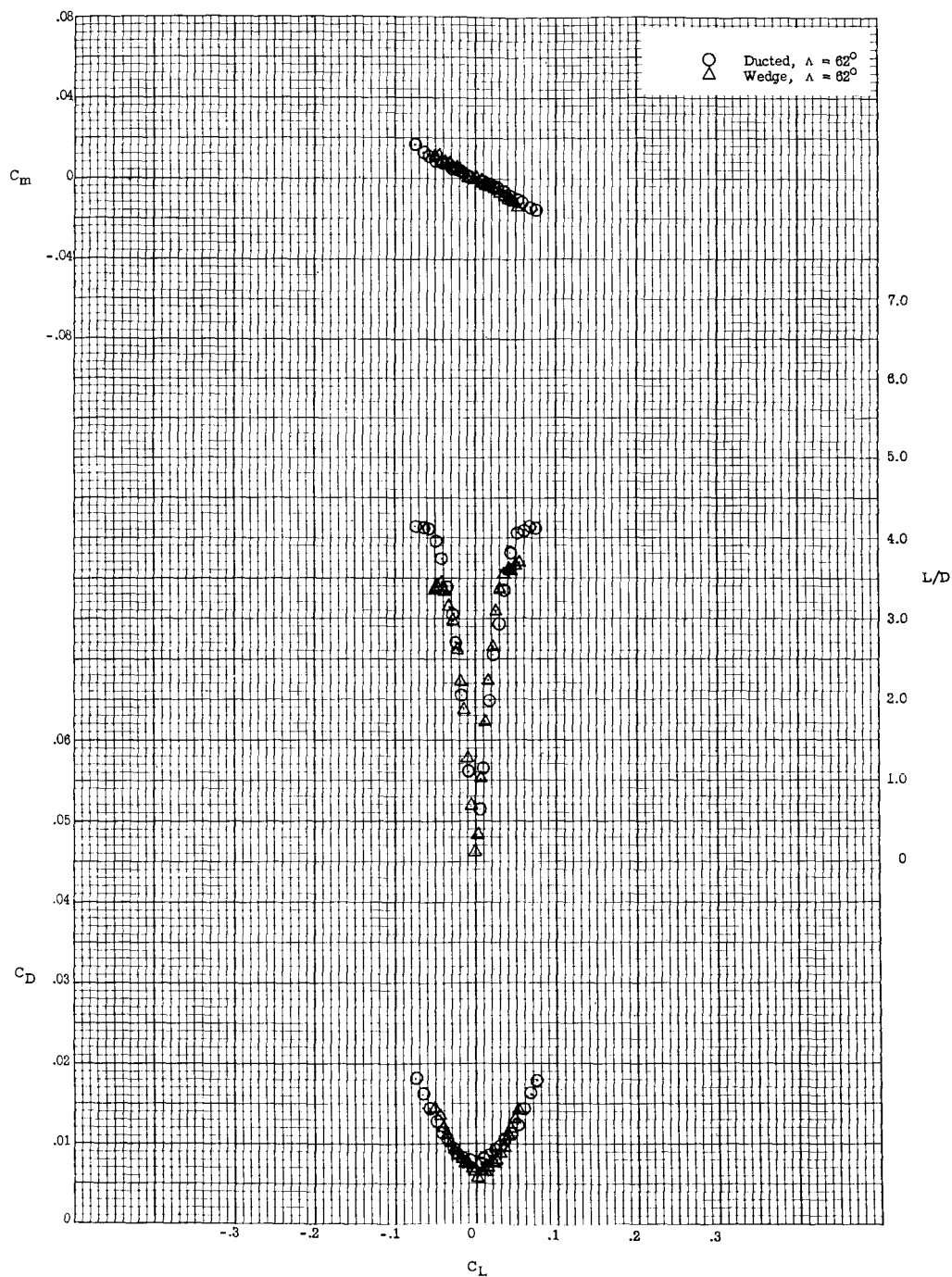


Figure 13.- Comparison of the configurations with canard off, forebody off, and wing off. $\beta = 0^\circ$; $M = 2.98$; $R = 3.5 \times 10^6$ based on wing mean aerodynamic chord.